JMEPEG (2012) 21:2594–2599
DOI: 10.1007/s11665-012-0275-3

1059-9495/$19.00

Hot Deformation Behavior of NiTiHf Shape Memory Alloy Under Hot Compression Test

Majid Belbasi, Mohammad T. Salehi, and Seyed Ali Asghar Akbari Mousavi

(Submitted December 8, 2011; in revised form May 27, 2012)

In this study, the hot deformation behavior of $Ni_{49}Ti_{36}Hf_{15}$ alloy was investigated. Compression tests were carried out at temperatures ranging from 800 to 1100 °C and at the strain rates of 0.001–1/s. The peak stress decreases with increasing deformation temperature and decreasing strain rate, a behavior which can be described by plotting the Zener-Hollomon parameter as a function of stress. It was realized that dynamic recrystallization (DRX) was responsible for flow softening. Most of the samples exhibited typical DRX stress-strain curves with a single peak stress followed by a gradual fall down stress. Microstructure evolution showed that new recrystallized grains formed in the vicinity of grain boundaries. The hyperbolic-sine-type constitutive model of $Ni_{49}Ti_{36}Hf_{15}$ alloy was obtained to provide basic data for determining reasonable hot-forming process. The activation energy for hot deformation of the $Ni_{49}Ti_{36}Hf_{15}$ alloy was close to 410 kJ/mol.

Keywords casting, intermetallics, rolling

1. Introduction

In the most common group of shape memory alloys (SMA), binary NiTi alloys, transformation temperatures hardly exceed 100 °C (Ref 1, 2). New NiTi-based high-temperature shape memory alloys, with transformation temperatures above 100 °C, have been recently developed. These alloys include NiTiX (X = Pt, Pd, Au, Zr, Hf) and have the potential of meeting the requirements for high-temperature applications. Among these alloys, NiTiHf alloys seem to be more practical for engineering applications, primarily due to high transformation temperatures, good thermal stability, and lower price compared with NiTiX (X = Pt, Pd, Au, Ref 1, 3-6). To date, several features such as phase composition, shape memory properties, martensitic transformation, mechanical properties, and aging of NiTiHf have been investigated (Ref 1, 3-13). The understanding of material behavior during hot deformation is of great importance in terms of industrial manufacturing processes such as hot rolling, forging, and extrusion. Furthermore, the constitutive equations are important tools for analyzing metal-forming processes. That is why many attempts have been made for developing constitutive equations of materials using the experimental data to model their hot deformation behavior (Ref 14). In spite of various studies conducted on the hot deformation of NiTi alloys, no research has been published on the hot compression behavior of the $Ni_{49}Ti_{36}Hf_{15}$ alloy. Therefore, the aim of the present research was first to study the hot deformation behavior of $Ni_{49}Ti_{36}Hf_{15}$ alloy. The second goal was to develop its constitutive equations which, to the best knowledge of the authors, were the first models in this regard.

This article is an invited paper selected from presentations at the International Conference on Shape Memory and Superelastic Technologies 2011, held November 6-9, 2011, in Hong Kong, China, and has been expanded from the original presentation.

Majid Belbasi, and **Mohammad T. Salehi**, School of Metallurgy and Materials Engineering, Iran University of Science and Technology, P.O. Box 16844, Tehran, Iran; and **Seyed Ali Asghar Akbari Mousavi**, School of Metallurgy and Materials Engineering, College of Engineering, University of Tehran, P.O. Box 11155-4563, Tehran, Iran. Contact e-mails: belbasi@iust.ac.ir, salehi@iust.ac.ir, and akbarimusavi@ut.ac.ir.

2. Experimental Procedure

$Ni_{49}Ti_{36}Hf_{15}$ ingot was prepared by vacuum induction melting (VIM) using 99.99% Ni, 99.7% Hf, and 99.97% Ti in a graphite crucible under the vacuum of 10^{-3} mbar. Homogenization of the ingot was carried out at 1000 °C for 20 h under vacuum following by quenching into water. Then, the cylindrical compression specimens with the diameter of 8 mm and the height of 12 mm were prepared from the homogenized ingot. Compression tests were carried out at temperatures ranging from 800 to 1100 °C, under strain rates of 0.001 to 1/s, by an Instron testing machine. The specimens were deformed under compression at a true strain of 0.7 and water cooled after deformation. In order to minimize the friction at the die-specimen interface, a mica foil was inserted between the die and the specimen. The load displacement data gathered from compression testing were then processed to plot the true stress-true strain curves. The data obtained from the stress-strain curves of hot compression tests were then used to determine the activation energy and Zener-Hollomon equation for the hot deformation of this alloy. The microstructures were studied by optical microscopy and energy-dispersive x-ray spectroscopy (EDS).

3. Results and Discussion

3.1 Flow Curves

The flow curve of $Ni_{49}Ti_{36}Hf_{15}$ alloy deformed at different temperatures and strain rates is shown in Fig. 1. It is obvious that

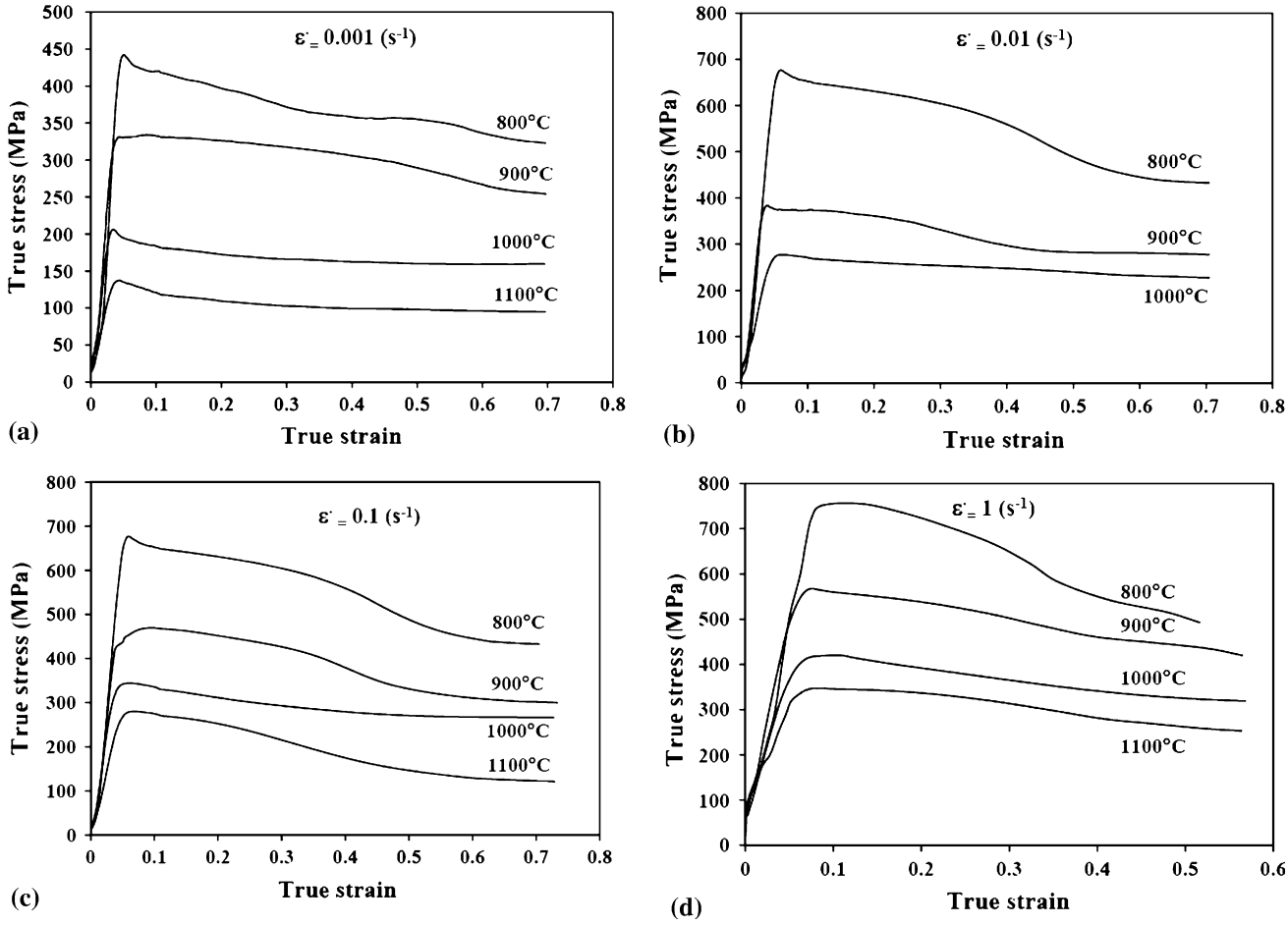

Fig. 1 Typical flow curve for $Ni_{49}Ti_{36}Hf_{15}$ alloy under different deformation temperatures with strain rates of (a) 0.001/s, (b) 0.01/s, (c) 0.1/s, and (d) 1/s

the true stress-strain curves exhibit single peaks at certain strains and then gradually decrease or even stay constant. According to Fig. 1, as usual, the flow stress decreases with increasing temperature and decreasing strain rate. Figure 2 shows the variation of peak stress with the strain rate at different temperatures. According to Fig. 2, with increasing the strain rate from 0.001 to 1/s, the flow stress increases from 446 to 776 MPa and 149 to 349 MPa at 800 and 1100 °C, respectively. The increase of the flow stress in the initial stage of the test, as expected, is due to work hardening. With increasing true strain, softening occurred and the stress reduced. The appearance of the peak stress showed typical characteristics of dynamic recrystallization (DRX) (Ref 14), suggesting that DRX is the dominating restoration mechanism during the hot deformation of $Ni_{49}Ti_{36}Hf_{15}$. As was expected, the effect of temperature increases on decline of flow stress was considerable. At higher temperatures, DRX dominated upon the work hardening and, as a result, at 1000 and 1100 °C, the flow stress was significantly lower.

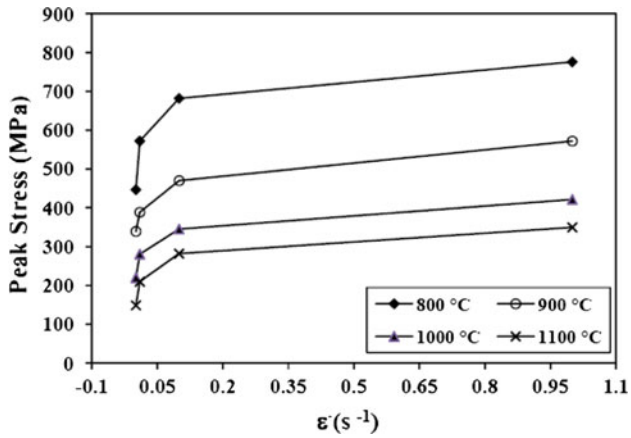

Fig. 2 Peak stress under different deformation temperatures with strain rates

3.2 Microstructure Observations

The onset of DRX is generally characterized by the appearance of a peak in flow curve (Fig. 1). This is the principle of DRX, which has been suggested and accepted widely by many famous scientists specializing in this subject, the primary of whom being, Poliak and Jonas (Ref 15, 16), Sakai and Jonas (Ref 16), and Luton and Sellars (Ref 17). However, the occurrence of DRX can also be shown by microstructural investigation. Figure 3 shows the microstructure of specimens that deformed at 1000 and 1100 °C and strain rates of 1 and 0.1/s. The figure clearly shows the new grains formed by DRX. A few recrystallized grains are observed in the vicinity of grain boundaries. Fine DRX grains nucleate almost exclusively at grain boundaries.

Deformation causes the initial grain to become elongated, inhomogeneous, and produce irregular, sharply edges, or toothed boundaries. By contrast, the recrystallized grains are normally homogenous, equiaxed, and regular in boundary and shape. Arrows in the figure show the new recrystallized grains.

Furthermore, as mentioned in the experimental procedure, the ingot was homogenized at 1000 °C for 20 h following by quenching into water. The performed heat treatment cannot result in producing the fine grains. Therefore, the new homogenous and equiaxed grains were the DRX grains which were smaller than the initial grains. Because of these reasons, the smaller grains shown by the arrow in Fig. 3 are DRX grains. Figure 4 displays the result of EDS analysis, which was used to figure out the nature of the second phase marked A, shown in Fig. 3. This phase contained 32.9 at.% Nickel, 58.5 at.% titanium, and 8.6 at.% hafnium. It was demonstrated that the second phase was close to the chemical composition of $(Ti,Hf)_2Ni$.

3.3 Constitutive Equations

In order to further investigate the hot deformation behaviors of $Ni_{49}Ti_{36}Hf_{15}$ alloy, it was necessary to study its deformation characteristics using constitutive equations. The data obtained from the stress-strain curves of hot compression tests were used for modeling the deformation behavior of $Ni_{49}Ti_{36}Hf_{15}$. Constitutive equations are commonly used to calculate the flow stress of a material during deformation (Ref 18-21). The basic equation is shown in Eq. 1. In this equation, the Zener-Hollomon parameter (Z) is the temperature compensated strain rate, Q is the activation energy of deformation, σ is the flow stress, and $\dot{\varepsilon}$ is the strain rate. Thus, far, three expressions of constitutive equations have been widely reported for modeling the material flow behavior in the literature. The power law (Eq 1) is preferred for creep; conversely, the exponential law (Eq 2) is only suitable for relatively low temperatures and high strain rates. However, the hyperbolic sine law (Eq 3) can be used for a wide range of temperatures and strain rates, which is utilized in this research

$$Z = \dot{\varepsilon}\exp(Q/RT) = f(\sigma) = \begin{cases} A'\sigma^{n'} & \text{(Eq 1)} \\ A''\exp(\beta\sigma) & \text{(Eq 2)} \\ A[\sinh(\alpha\sigma)]^n & \text{(Eq 3)} \end{cases},$$

where A, A', A'', n, n', β, and α ($=\beta/n'$) are material constants.

3.4 Determining Hot Working Constants

To determine the constants by taking the natural logarithm from each side of the resulting equations, the following expressions could be derived for the peak stress:

$$\ln\dot{\varepsilon} + Q/RT = \ln A' + n'\ln\sigma_p \quad \text{(Eq 4)}$$

$$\ln\dot{\varepsilon} + Q/RT = \ln A'' + \beta\sigma_p \quad \text{(Eq 5)}$$

$$\ln\dot{\varepsilon} + Q/RT = \ln A + n\ln[\sinh(\alpha\sigma_p)] \quad \text{(Eq 6)}$$

At the constant deformation temperature, the partial differentiation of Eq 4, 5, and 6 yields the following equations, respectively:

$$n' = [\delta\ln\dot{\varepsilon}/\delta\ln\sigma_p]_T \quad \text{(Eq 7)}$$

$$\beta = [\delta\ln\dot{\varepsilon}/\delta\sigma_p]_T \quad \text{(Eq 8)}$$

$$n = [\delta\ln\dot{\varepsilon}/\delta\ln\{\sinh(\alpha\sigma_p)\}]_T \quad \text{(Eq 9)}$$

It follows from these expressions that the slope of the plot of $\ln\dot{\varepsilon}$ against $\ln\sigma_p$, the slope of the plot of $\ln\dot{\varepsilon}$ against σ_p, and the slope of the $\ln\dot{\varepsilon}$ against sinh ($\alpha\sigma_p$) can be used for obtaining the values of n', β, and n, respectively. These plots are shown in Fig. 5(a), (b), and (c). respectively. The linear regression of these data resulted in the average values of 10.9, 0.029, and 7.9 for n', β, and n, respectively. According to these data, the value of $\alpha = \beta/n' = 0.0026$.

To calculate the activation energy, the partial differentiation of Eq 6 at a constant strain rate yields the following equation:

$$Q = Rn[\delta\ln\{\sinh(\alpha\sigma_p)\}/\delta(1/T)]_{\dot{\varepsilon}} \quad \text{(Eq 10)}$$

It is obvious from this expression that the slope of the plot of ln {sinh($\alpha\sigma_p$)} against the reciprocal of the absolute temperature can be used for calculating the value of Q (this plot is shown in Fig. 6). The linear regression of this data resulted in the average value of 410 kJ/mol for the activation energy from Eq 10. According to Fig. 7, analysis of the correlation coefficient (R^2) of this regression value reveals that Eq 10 is a suitable fit with the experimental data. Therefore, the activation energy of hot working was considered to be 410 kJ/mol.

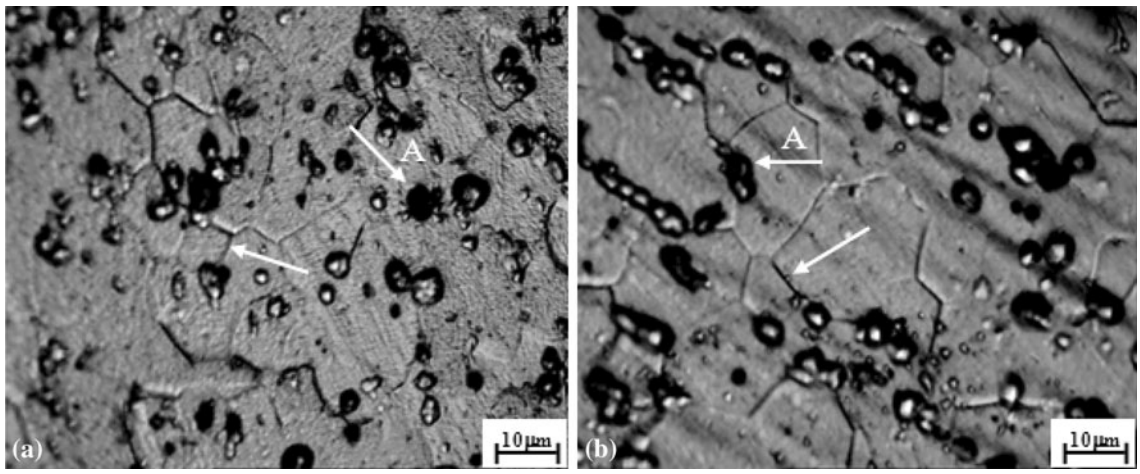

Fig. 3 Typical microstructure of the $Ni_{49}Ti_{36}Hf_{15}$ alloy deformed at (a) 1000 °C and 1/s and (b) 1100 °C and 0.1/s

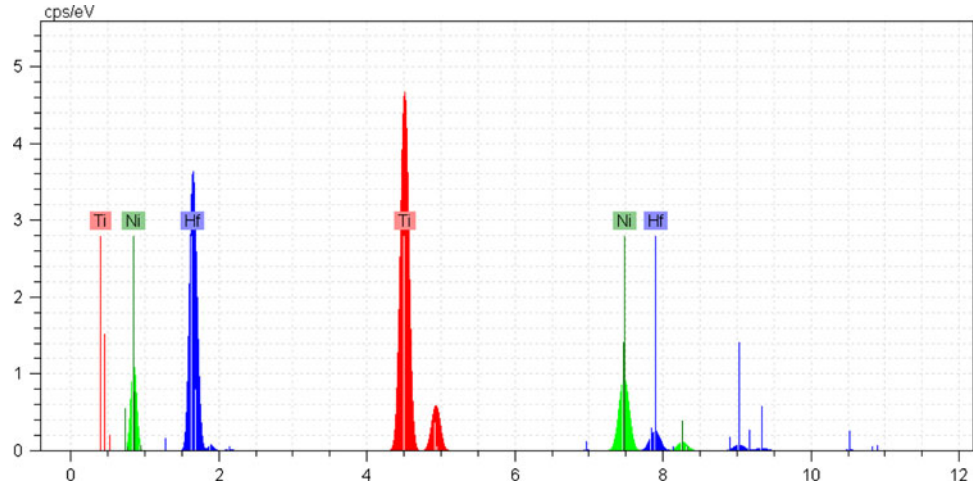

Fig. 4 Typical EDS analysis of the second phase marked A, shown in Fig. 3

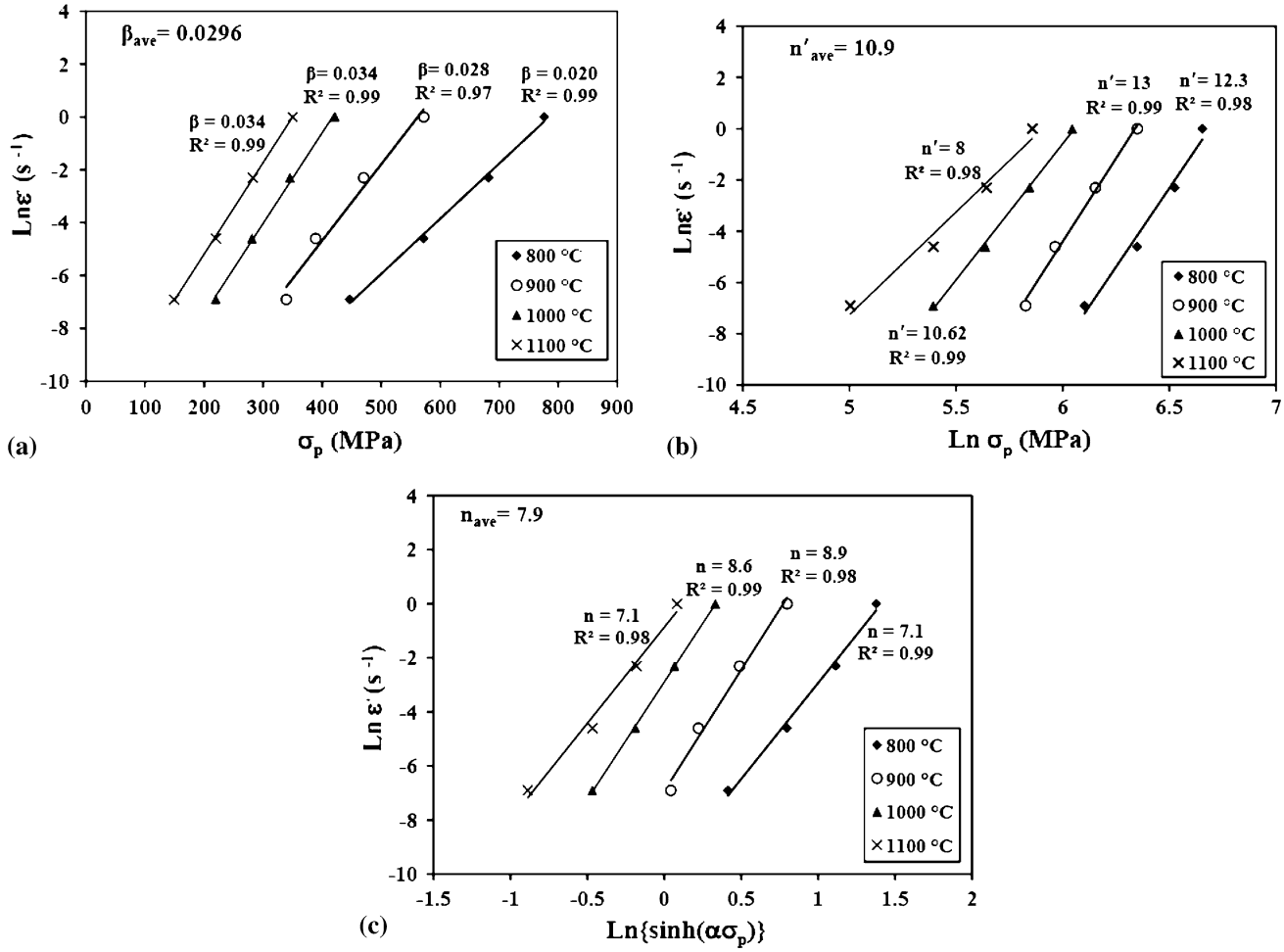

Fig. 5 Plots used for calculation of (a) β, (b) n', and (c) n

According to Fig. 3 and 4 and the EDS result of Ref 14, the type of second phase particles of NiTi binary alloy was different from that of the NiTiHf alloys. The magnitude of flow stress achieved from the NiTiHf alloy was almost three folds of that of Ref 14. The increase in flow stress of the NiTiHf alloy can be attributed to (Ti,Hf)2Ni second phase particles. The presence of strengthening precipitates interacting with dislocations is known to cause an increase of the activation energy and stress exponent experimental values. In this sense, the higher value of activation energy obtained in Ni49Ti36Hf15 in

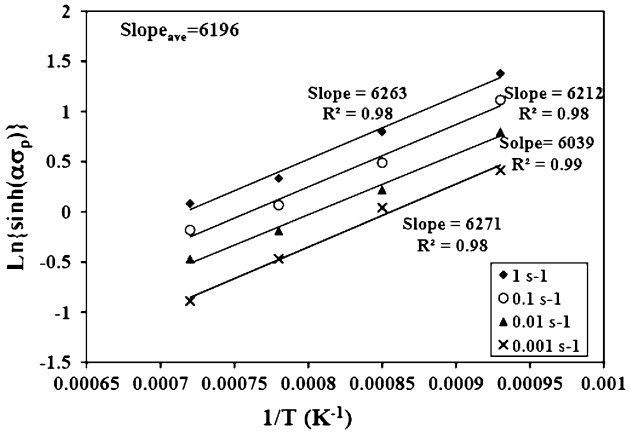

Fig. 6 Plot of $\ln\{\sinh(\alpha\sigma_p)\}$ against the reciprocal of absolute temperature

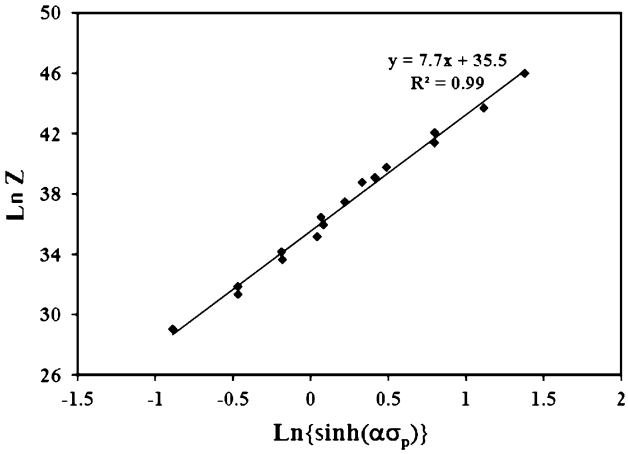

Fig. 7 Plot of $\ln Z$ vs. $\ln\{\sinh(\alpha\sigma_p)\}$

comparison with other NiTi alloys can be attributed to the particle strengthening effect.

3.5 Peak Stress as a Function of the Zener-Hollomon Parameter

According to Eq 3, the plot of $\ln Z$ versus $\ln\{\sinh(\sigma_p)\}$ can be used for finding the relationship between Z and σ_p. The corresponding curve is shown in Fig. 7 and the resultant regression equation with various constants is as follows:

$$\ln Z = \ln A + n\ln\left[\sinh\left(\alpha\sigma_p\right)\right]$$

$$Z = \dot{\varepsilon}\exp(410000/RT) = 2.66 \times 10^{15}[\sinh(0.0029\sigma)]^{7.9} \quad \text{(Eq 11)}$$

In accordance with Fig. 7, the hyperbolic sinus equation (Eq 11) has the correlation coefficient of 0.99. Therefore, the hyperbolic sinus equation is the best constitutive equation to describe the hot deformation behavior of $Ni_{49}Ti_{36}Hf_{15}$. The hot deformation behavior of $Ni_{49}Ti_{36}Hf_{15}$ can be expressed as Eq 12, as a result of the rearrangement of Eq 11.

$$\dot{\varepsilon} = 2.66 \times 10^{15}\left[\sinh\left(0.0029\sigma_p\right)\right]^{7.9}\exp(-410000/RT) \quad \text{(Eq 12)}$$

4. Conclusion

This study investigated the hot deformation behavior of the $Ni_{49}Ti_{36}Hf_{15}$ alloy as an attractive candidate for SMAs which are used at high temperatures due to their high transformation temperatures. The study was conducted to develop the constitutive equations for the $Ni_{49}Ti_{36}Hf_{15}$ alloy. The constitutive equations can be used for analyzing and studying the hot workability of this alloy. The flow stress behavior of $Ni_{49}Ti_{36}Hf_{15}$ shape memory alloy was shown to be very temperature- and strain rate-sensitive. The increase of strain rate intensified the flow stress and the increase in temperature significantly decreased the flow stress. Work hardening determined the rapid increase in flow stress observed in the early stage of the experiments. With increasing the true strain, the stress-stain curve reduced due to softening. The appearance of peak stress and formation of new grain in the vicinity of grain boundaries showed the typical characteristics of DRX. It was explained that, to calculate the correct value of activation energy during hot working, one of the three expressions of Z, namely, the power law, exponential law, and hyperbolic sinus law, could be used. For $Ni_{49}Ti_{36}Hf_{15}$ alloy, the hyperbolic sinus law was found to be the appropriate relation, which resulted in the activation energy value of 410 kJ/mol. According to the analysis of hot deformation behavior of $Ni_{49}Ti_{36}Hf_{15}$ in this work, the following hyperbolic sinus equation was achieved.

$$\dot{\varepsilon} = 2.66 \times 10^{15}\left[\sinh\left(0.0029\sigma_p\right)\right]^{7.9}\exp(-410000/RT)$$

References

1. X.L. Meng, Y.F. Zheng, Z. Wang, and L.C. Zhao, Effect of Aging on the Phase Transformation and Mechanical Behavior of $Ti_{36}Ni_{49}Hf_{15}$ High Temperature Shape Memory Alloy, *Scr Mater*, 2000, **42**, p 341–348
2. X.L. Meng, Y.F. Zheng, Z. Wang, W. Cai, and L.C. Zhao, Phase Transformation and Precipitation in Aged Ti-Ni-Hf High-Temperature Shape Memory Alloys, *Mater. Sci. Eng., A*, 2006, **438**(440), p 666–670
3. G.S. Firstov, J.V. Humbeeck, and Y.N. Koval, High-Temperature Shape Memory Alloys: Some Recent Developments, *Mater. Sci. Eng., A*, 2004, **378**, p 2–10
4. P.L. Potapov, A.V. Shelyakov, A.A. Gulyaev, E.L. Svistunova, N.M. Matveeva, and D. Hodgson, Effect of Hf on the Structure of Ni-Ti Martensitic Alloys, *Mater. Lett.*, 1997, **32**, p 247–250
5. X.L. Meng, W. Cai, L.M. Wang, Y.F. Zheng, L.C. Zhao, and L.M. Zhou, Microstructure of Stress-Induced Martensite in a Ti-Ni-Hf High Temperature Shape Memory Alloy, *Scr Mater*, 2001, **45**, p 1177–1182
6. W. Cai, X.L. Meng, and L.C. Zhao, Recent Development of TiNi-Based Shape Memory Alloys, *Curr. Opin. Solid State Mater. Sci.*, 2005, **9**, p 296–302
7. Y.Q. Wang, Y.F. Zheng, and L.C. Zhao, The Tensile Behavior of $Ti_{36}Ni_{49}Hf_{15}$High Temperature Shape Memory Alloy, *Scr Mater*, 1999, **40**, p 1327–1331
8. C. Craig Wojcik, Properties and Heat Treatment of High Transition Temperature Ni-Ti-Hf Alloys, *Mater. Eng. Perform.*, 2009, **18**, p 511–516
9. X.L. Meng, W. Cai, Y.D. Fu, Q.F. Li, J.X. Zhang, and L.C. Zhao, Shape-Memory Behaviors in an Aged Ni-Rich TiNiHf High Temperature Shape-Memory Alloy, *Intermetallics*, 2008, **16**, p 698–705
10. P.E. Thoma and J.J. Boehm, Effect of Composition on the Amount of Second Phase and Transformation Temperatures of NixTi90-xHf10 Shape Memory Alloys, *Mater. Sci. Eng., A*, 1999, **273**, p 385–389
11. Y. Tong, F. Chen, B. Tian, and Y. Zheng, Microstructure and Martensitic Transformation of Ti49Ni51-xHfx High Temperature Shape Memory Alloys, *Mater. Lett.*, 2009, **63**, p 1869–1871

12. S. Besseghini, E. Villa, and A. Tuissi, Ni-Ti-Hf Shape Memory Alloy: Effect of Aging and Thermal Cycling, *Mater. Sci. Eng., A*, 1999, **273**, p 390–394
13. S. Han, W. Zou, S. Jin, Z. Zhang, and D. Yang, The Studies of the Martensite Transformations in a $Ti_{36}Ni_{49}Hf_{15}$ Alloy, *Scr Mater*, 1995, **32**, p 1441–1446
14. K. Dehghani and A.A. Khamei, Hot Deformation Behavior of 60Nitinol (Ni60 wt%-Ti40 wt%) Alloy Experimental and Computational Studies, *Mater. Sci. Eng., A*, 2010, **527**, p 684–690
15. E.I. Poliak and J.J. Jonas, Initiation of Dynamic Recrystallization in Constant Strain Rate Hot Deformation, *ISIJ Int.*, 2003, **43**, p 684–691
16. T. Sakai and J.J. Jonas, Dynamic Recrystallization: Mechanical and Microstructural Considerations, *Acta Metall.*, 1984, **32**, p 189–209
17. M.J. Luton and C.M. Sellars, Dynamic Recrystallization in Nickel and Nickel-Iron Alloys During Hot Temperature Deformation, *Acta Metall.*, 1969, **17**, p 1033–1043
18. X. He, Zh Yu, and X. Lai, A Method to Predict Flow Stress Considering Dynamic Recrystallization During Hot Deformation, *Mater. Sci.*, 2008, **44**, p 760–764
19. H.J. Mcqueen and N.D. Ryan, Constitutive Analysis in Hot Working, *Mater. Sci. Eng., A*, 2002, **322**, p 43–63
20. Y.C. Lin, M.S. Chen, and J. Zhong, Constitutive Modeling for Elevated Temperature Flow Behavior of 42CrMo Steel, *Mater. Sci.*, 2008, **42**, p 470–477
21. D. Samantary and S. Mandal, Constitutive Analysis to Predict High Temperature Flow Stress in Modified 9Cr-1Mo Steel, *Mater. Des.*, 2010, **31**, p 981–984